



RESEARCH ARTICLE

A class of spatial remote center-of-motion mechanisms and its forward kinematics

Yuan Bian¹, Jianchang Zhao^{1,2} , Jinhua Li^{1,2}, Guowu Wei³  and Jianmin Li^{1,2,*}

¹Key Laboratory of Mechanism Theory and Equipment Design, Ministry of Education, Tianjin, China, ²Institute of Medical Robotics and Intelligent Systems of Tianjin University, Tianjin, China, and ³School of Science, Engineering, and Environment, University of Salford, Salford, UK

*Corresponding author. E-mail: mjli@tju.edu.cn

Received: 24 December 2021; **Revised:** 2 June 2022; **Accepted:** 27 June 2022; **First published online:** 27 July 2022

Keywords: minimally invasive surgical robot, remote center-of-motion mechanism, forward kinematics

Abstract

Robot-assisted minimally invasive surgery (MIS) has shown tremendous advances over the traditional technique. A crucial challenge for developing a MIS robot is the kinematic design of the remote center-of-motion (RCM) mechanism. In this paper, a class of spatial RCM mechanism is analyzed. They are obtained by generating virtual parallelograms. The main process is to construct a line that passes through a fixed point under the mechanical constraint. The axis of the surgical tool is then constrained to parallel with that line. Hence, due to the geometrical feature of the parallel lines, the axis of the surgical tool will always pass through a fixed point, i.e., the RCM point. Due to the specially designed structure, the fixed point does not need to be physically belonging to the mechanism. The geometrical analysis method is employed to obtain the closed-form solution of the forward kinematics of the proposed mechanisms. Due to the high load capacity of parallel mechanism, the robots based on the proposed RCM mechanisms have promising applications as an external positioner to be used in robotic single-port surgeries.

1. Introduction

Minimally invasive surgery (MIS) is increasingly popular nowadays and has received lots of support and favor from surgeons and patients. It is performed by inserting long, thin surgical tool into the patient's body through small incisions. Operations are carried out by manipulating the tool handles from outside of the body cavity. The benefits of this kind of operation to patients include less pain and blood loss, small scars, and shorter hospital stays. However, due to the motion constraint imposed upon the surgical tool by the almost stationary incisions, several drawbacks still exist in the current MIS technique. These include limited dexterity, restricted vision, and uncoordinated hand-eye motion. Thus, the MIS demands considerably more training and practice for surgeons compared to the traditional open surgeries.

The effectiveness of MIS can be significantly improved by introducing robotic technology. It can overcome the drawbacks involved in MIS, and it has led to momentous change in and generates a tremendous impact on surgery [1]. The da Vinci surgical robotic system is the most successful commercial system, which has received clearance from the US Food and Drug Administration [2]. Regarded as a milestone, it is well received by clinical community. Currently, more than 5000 da Vinci robots are used in hospitals and medical centers over the world. The great success of da Vinci surgical system has stimulated the research of robot-assisted MIS technology in both engineering and clinical fields.

The kinematic design is one of the most important phases in a MIS robot design. Due to the fixed incision, DOFs of the tool are restricted to four (the Open & Close is not included) as shown in Fig. 1. They are rotation 1, rotation 2, rotation 3, and the translation. For safety reasons, the rotations of the surgical tool should always pivot against the incision point, while the translational motion should always along the line that passes through the incision point. The direction of the translation is determined by

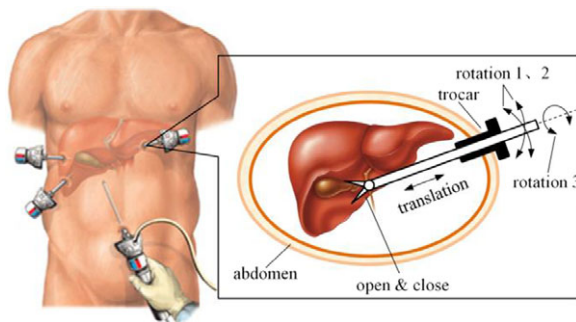


Figure 1. The incision point constraint in the MIS surgery [3].

rotation 1 and rotation 2. This kind of motion is called the remote center-of-motion (RCM), which is the fundamental requirement of a MIS robot.

Current methods to make the MIS robot pass through the incision point include (a) controlling redundant joints, such as the MIRO system developed by DLR [4] and the improved version of PARAMIS robot [5–7]; (b) adding passive joints, such as the Zeus system [8] and the MicroHand S robot [9]; and (c) mechanically constrained structure, such as the da Vinci system. The robot based on the first method can provide high stiffness but is considered unsafe in a surgery [10]. Which one is safer between the latter two methods is still in debates, but the safety of the adding passive joints method is achieved at the expense of compromising the motion accuracy and stiffness [11].

For the mechanically constrained structure, the introduction of a circular arc is probably the structurally simplest way to generate an RCM. The movement of a slider on a spherical arc is a 1-DOF remote center of motion. If the arc is driven by a revolute joint whose axis passes through the RCM, then another rotational DOF is added. The robotic camera holder “freehand” [12] and the light weight robotic scope holder “ViKY” [13] are developed based on this principal. If two or more links are connected serially by rotation joints with all axes intersecting at a single point, then the links can rotate on a sphere about this point. If a shaft is fixed on the tip of the last linkage, it will be forced to pass through the center of the sphere, which is the RCM. A portable MIS robot [14], the force reflecting robot MC²E [15, 16], and the Raven robot [17] are based on this method. Zoppi et al. proposed a class of 4-DOF parallel RCM manipulators and presented its analytical kinematic models and geometries [18].

The double parallelogram mechanism is the most widely used RCM mechanism in MIS robots [19–26], including the da Vinci surgical system which has been successfully applied in many robot-assisted MIS fields. Zong et al. proposed a type synthesis method to generate parallelogram based 1-DOF RCM mechanisms [27]. Several novel mechanisms were developed based on this principle. The deformation types of double parallelogram are important in this context and were analyzed in [28, 29]. The typical feature of MIS robots based on this kind of mechanisms is that they have two rotational DOFs about two orthogonal axes at the RCM point [30]. A spatial 3-DOF RCM mechanism, which is also based on parallelograms, was proposed by Ricardo et al. [31]. Due to its large volume, it is difficult to arrange several around the patient table. However, it can be used as an external positioner for assisting single port laparoscopic surgeries. For spatial RCM mechanisms, Li et al. have proposed a type synthesis method based on intersecting movable planes to generate novel RCM mechanisms [32], Kuo and Dai proposed a fully decoupled 4-DOF RCM mechanism for MIS [33].

It needs to point out that an active prismatic joint is needed to drive the tool move in-out of the patient’s body, whether a circular arc or double parallelogram is used. In the prototype design, the active prismatic joint generally needs to use ball screw. Therefore, for the same scale workspace, the active prismatic joint has heavier mass, larger volume, and less flexibility than the active rotating joint. And it is difficult to realize the integration of driving parts on the static platform, and the increase of motion inertia will lead to the increase of driving force. This requirement makes the transmission system complex and reduces the back-drivability of the surgical robot. Under this condition, a class of 2-DOF planar RCM

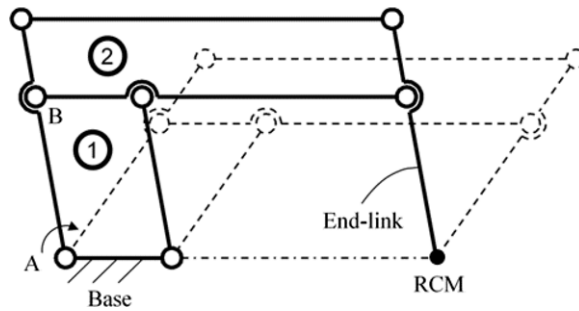


Figure 2. The double parallelogram mechanism.

mechanisms is proposed by constructing virtual parallelograms [3]. Considering that the actuated joints of the obtained mechanisms are revolute joints, they have better back-drivability and flexibility than the standard double parallelogram. Therefore, the proposed mechanisms have great application potential in MIS robots.

In this paper, the three-dimensional version of the above mentioned 2-DOF planar RCM mechanism is investigated. Compared to the existing spherical parallel mechanisms, the advantage of the proposed design is that each of spatial RCM mechanism has a translational motion that passes through the RCM. This can be used to driven the surgical tool move in-out of the patient's body cavity. Other scholars have proposed RCM mechanisms which can realize translational degrees of freedom. Long et al. proposed an RCM mechanism without active prismatic joint [34]. Although the structure of the mechanism in reference [34] is simple, it does not realize the integration of the motor on the static platform, and the stiffness perpendicular to the paper direction is low. In contrast, the three actuators of the mechanism proposed in this paper are fixed on the static platform, which is easy to realize modular design. In addition, the overall structure has the characteristics of high stiffness and isotropy. The basic principle, the sufficient conditions that make the mechanism be spatial RCM mechanism, and the forward kinematics are analyzed in the following sections.

2. Double parallelogram mechanism

The double parallelogram is the most widely used mechanism in MIS robots. It is a 1-DOF RCM mechanism which is formed by combining two parallelogram linkages together, as shown in Fig. 2. This constraint makes the movement of a part of the mechanism, i.e., the End-link shown in the figure, perform pure rotation around a fixed point which is not physically belonging to the mechanism, this is the RCM point.

By investigating the constraint feature of the double parallelogram, it can be seen that the End-link is always parallel to link AB due to the constraint of the second parallelogram labeled in Fig. 2. The motion of the two horizontal links of the second parallelogram is purely translational motion due to the constraint of the first parallelogram labeled in Fig. 2. In such a construction, since one end of link AB is installed on the base through a revolute joint, i.e., joint A, end-point of the entangled End-link always passes through an RCM (see Fig. 2) when the mechanism works. Inspired by this design, a method that can generate new RCM mechanisms raises. In this method, we construct two lines, connected by a parallelogram, one of which passes through a fixed point under the physical constraint. Then if the motion of the parallelogram is restricted to be pure translation, the other line will always pass through a virtually fixed point that needs not to be physically belonging on the mechanism. Such a point is coined the RCM point. Based on this idea, the authors proposed a class of 2-DOF planar RCM mechanisms [3], and several other kinds of 2-DOF planar RCM mechanisms were developed based on the consistent method [35–38]. Based on our previous work, in this paper, we proposed a 3-DOF spatial RCM mechanism.

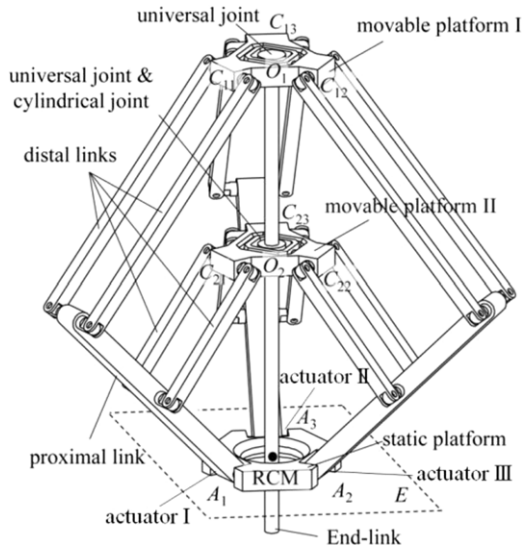


Figure 3. A spatial 3-DOF double-Delta mechanism with RCM.

3. A 3-DOF spatial RCM mechanism

Based on the construction of RCM mechanisms in parallelogram mechanisms in form, we aim to construct spatial RCM mechanisms according to the same design principle.

3.1. Design of a 3-DOF spatial double-Delta mechanism with RCM

As mentioned above, a key step to generate new RCM mechanisms is to find a suitable mechanism that can drive a parallelogram to execute pure translation. The Delta mechanism proposed by Clavel [35] is the most famous parallel mechanism that can generate purely translational motion. This feature makes the mechanism suitable as the basis to generate spatial RCM mechanisms.

Based on the mechanism constructing method proposed in [3], and the principle proposed in Section 2, a kind of spatial mechanism based on the Delta mechanism is constructed in this paper, as shown in Fig. 3. From the figure, it can be seen that this spatial mechanism contains two layers of Delta-like linkages. In this design, to make the motions of the two Delta linkages coupled with each other, the parallelograms in the two Delta linkages share the same proximal linkage. Three platforms, i.e., movable platform I, movable platform II, and static platform are used in the mechanism. To fulfill the mobility constraint, the End-link is mounted on the movable platform I through a universal joint and connected with the movable platform II via a universal joint together with a cylindrical joint. The actuators used for driving the mechanism can be set stationary on the static platform, as shown in Fig. 3. The End-link is the end-effector of the proposed double-Delta mechanism with remote center of motion. Different with the common Delta mechanism in the literature, in this design, the three proximal links and the three groups of distal links in each Delta linkage have different lengths, and the dimensions of the three platforms, the static platform and the two movable platforms are identical.

There are $n = 36$ links and $j = 42$ joints (including 39 revolute joints, 2 universal joints and 1 cylindrical joint) in the proposed mechanism. Through the test in the model, it is found that once any joint constraint is removed, the remote center of motion cannot be realized, so there is no redundant constraint. Therefore, according to the Grübler–Kutzbach formula [38], the mobility of the mechanism is

$$m = \lambda(n - j - 1) + \sum_{i=1}^j f_i = 6(36 - 42 - 1) + 39 + 2 + 2 + 2 = 3 \quad (1)$$

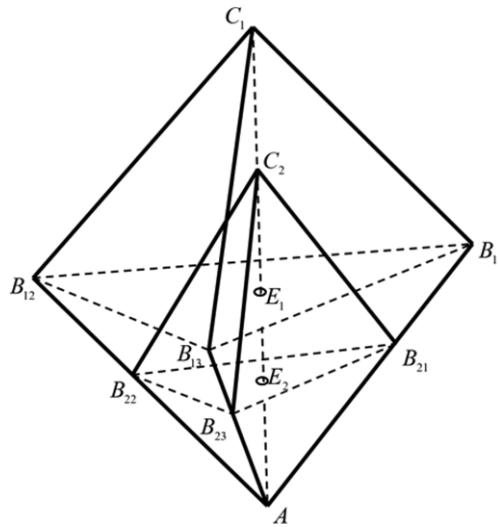


Figure 4. The schematic model of the mechanism under the first condition.

where m denotes the mobility of the mechanism and λ is the dimension of the space in which the mechanism is presented, $\lambda = 6$ for spatial mechanism and $\lambda = 3$ for planar and spherical mechanisms.

3.2. Conditions for remote center of motion

To realize remote center of motion for the End-link of the proposed mechanism, there are two conditions need to be satisfied: first, lengths of all the proximal links and lengths of all the distal links in each Delta linkage are same, respectively; and second, the corresponding distal links in the two Delta linkages are parallel with each other. Based on these two conditions, kinematic analysis of the mechanism will be investigated in Section 4 to verify whether the mechanism can execute the RCM motion.

The schematic model of the mechanism is shown in Fig. 4, from the first condition, it is expected that the two movable platforms, simplified as points C_1 and C_2 in the figure (it is noted that the static platform is also simplified as a point A), will have pure translational motion due to the constraints of the parallelograms.

From Fig. 4, it can be seen that line C_1E_1 is the normal line of the plane formed by points B_{11} , B_{12} , and B_{13} (denoted as $\pi B_{11}B_{12}B_{13}$), and line C_2E_2 is the normal line of the plane formed by points B_{21} , B_{22} , and B_{23} (denoted as $\pi B_{21}B_{22}B_{23}$). Then, based on the conditions that $C_1E_1 \perp \pi B_{11}B_{12}B_{13}$ and $C_1B_{11} = C_1B_{12} = C_1B_{13}$, it has

$$E_1B_{11} = E_1B_{12} = E_1B_{13} \tag{2}$$

thus point E_1 is the circumcenter of triangle $\delta B_{11}B_{12}B_{13}$.

Similarly, with the conditions that $C_2E_2 \perp \pi B_{21}B_{22}B_{23}$ and $C_2B_{21} = C_2B_{22} = C_2B_{23}$, it yields

$$E_2B_{21} = E_2B_{22} = E_2B_{23} \tag{3}$$

hence, point E_2 is the circumcenter of triangle $\delta B_{21}B_{22}B_{23}$.

Similarly, we can prove that line AE_1 is perpendicular to plane $\pi B_{11}B_{12}B_{13}$ with point E_1 and line AE_2 is orthogonal with plane $\pi B_{21}B_{22}B_{23}$ with point E_2 . With these results, it can be seen that the two lines, i.e., AE_1 and C_1E_1 , are both perpendicular to the plane $\pi B_{11}B_{12}B_{13}$, which means lines AE_1 and C_1E_1 are collinear. Similarly, it can be concluded that lines AE_2 and C_2E_2 are collinear.

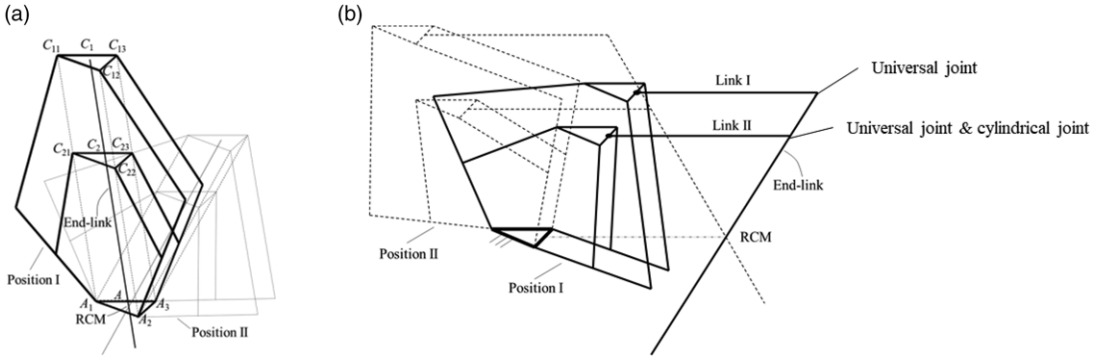


Figure 5. The mechanism can execute RCM motion under the mentioned constraint.

Further, considering that the lengths of the corresponding links in the two Delta linkages are the same, there exist the following relations:

$$\frac{\overline{AB_{21}}}{\overline{AB_{11}}} = \frac{\overline{AB_{22}}}{\overline{AB_{12}}} \text{ and } \frac{\overline{AB_{21}}}{\overline{AB_{11}}} = \frac{\overline{AB_{23}}}{\overline{AB_{13}}} \tag{4}$$

which leads to the relations that $B_{11}B_{12}/B_{21}B_{22}$ and $B_{11}B_{13}/B_{21}B_{23}$, and thus $\pi B_{11}B_{12}B_{13}/\pi B_{21}B_{22}B_{23}$. Moreover, with the relations that $AC_1 \perp \pi B_{11}B_{12}B_{13}$ and $AC_2 \perp \pi B_{21}B_{22}B_{23}$, it can be found that lines AC_1 and AC_2 are collinear.

Therefore, from the above derivation, it can be found that the three points A, C₁, and C₂ in Fig. 4 are collinear. Further, since points A, C₁, and C₂ in Fig. 4 stand for the corresponding static and movable platforms in Fig. 3, there exist the relations that the three points C₁₁, C₂₁, and A₁ in one branch of the mechanism (see in Fig. 3) are always collinear. Similarly, points C₁₂, C₂₂, and A₂ and points C₁₃, C₂₃, and A₃ in the other two branches are also collinear, respectively.

Considering the above relations, in the mechanism, three generalized double parallelograms can be formed denoting as $P_1: C_{12}A_2A_3C_{13}$ & $C_{22}A_2A_3C_{23}$, $P_2: C_{11}A_1A_2C_{12}$ & $C_{21}A_1A_2C_{22}$, and $P_3: C_{11}A_1A_3C_{13}$ & $C_{21}A_1A_3C_{23}$ as shown in Fig. 5(a). Then referring to Fig. 5(a), the End-link that passes through points C₁, C₂, and A is parallel with lines A₁C₁₁, A₂C₁₂, and A₃C₁₃ and always has point A (which is the circumcenter of triangle $\Delta A_1A_2A_3$) as its remote center of motion. The remote center of motion is visually located in the center of the static platform, but does not need to be supported by physical links or joints. The operation space can be reserved by expanding the size of the static platform, so that human surgeons can clearly enter the incision. Based on the above constraints, the size of platform C1 can be kept unchanged and the size of platform C2 and base a can be expanded in proportion to ensure that the volume is not excessively expanded. It is important to point out that the End-link can also be located outside of the mechanism, as illustrated in Fig. 5(b). In this configuration, two links of equal length, i.e., Link I and Link II, are fixed on the movable platform I and movable platform II, respectively. The joint connect Link I and the End-link is a universal joint and a universal joint and a cylindrical joint are adopted to connect Link II and the End-link. For practical application, if the mechanism is to be used as the end effector of a surgical robot, for the case in Fig. 5(b), the mechanism body can be set away from the patient, making the mechanism better adapted to the surgical environment.

The second condition is that the corresponding distal links in the two Delta linkages are parallel with each other. This condition will secure that the three points A, C₁, and C₂ are collinear. To provide this, we simplify the kinematic model of the mechanism into a schematic model as shown in Fig. 6 and assume that three points A, C₁, and C₂ are not collinear. Based on the condition, it has lines B₂₁C₂ and B₁₁C₁ are parallel with each other, and lines AC₂ and B₁₁C₁ are in the same plane. Then point C'₁ is used to denote the intersection of the extension of the line AC₂ and the line B₁₁C₁ under the above assumption.

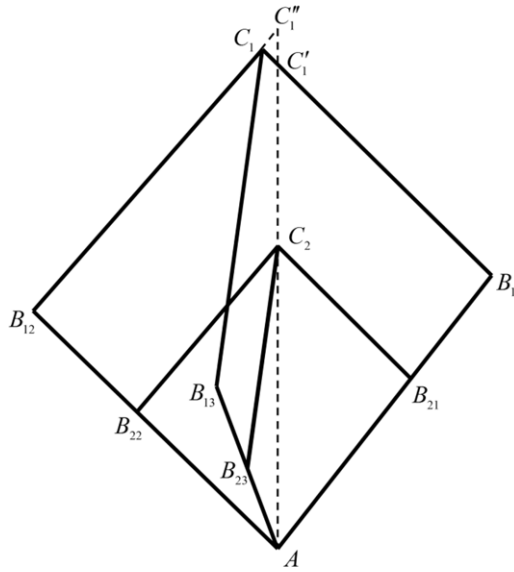


Figure 6. The schematic model of the mechanism under the second condition.

The mathematical description of the studied condition is

$$\begin{cases} \frac{AB_{21}}{AB_{11}} = \frac{AB_{22}}{AB_{12}} = \frac{AB_{23}}{AB_{13}} = k & (0 < k < 1) \\ B_{2j}C_2 // B_{1j}C_1 & j = 1, 2, 3 \end{cases} \quad (5)$$

Based on the intercept theorem of parallel lines, we have

$$\frac{AB_{21}}{AB_{11}} = \frac{AC_2}{AC'_1} \quad (6)$$

Further, considering that the line $B_{22}C_2$ is parallel with the line $B_{12}C_1$, these two lines can form a plane, i.e., the plane $\pi C_1 B_{12} B_{22} C_2$. Obviously, point A and point C_2 locate in that plane. It can be seen that line $B_{12}C_1$ and line AC_2 are the two intersecting lines within that plane. Let us assume that the intersecting point of the two lines is point C'_1 , as shown in figure. Then, based on the same theorem, it yields

$$\frac{AB_{22}}{AB_{12}} = \frac{AC_2}{AC'_1} \quad (7)$$

According to Eq. (5) throughout Eq. (7), it is straightforward to find that

$$\frac{AC_2}{AC'_1} = \frac{AC_2}{AC''_1} \quad (8)$$

Since both of the points C'_1 and C''_1 are on the extension of line AC_2 , Eq. (8) implies that points C'_1 and C''_1 are coincide. This result indicates that there is a unique intersecting point among three lines AC_2 , $B_{12}C_1$, and $B_{11}C_1$. Since C_1 is the intersecting point of lines $B_{12}C_1$ and $B_{11}C_1$, the above-mentioned unique intersecting point is point C_1 . Similarly, it can be found that point C_1 is also the intersecting point of lines AC_2 and $B_{13}C_1$. From above analysis, it can be proved that under the second condition, the three points A , C_1 , and C_2 are collinear.

Further, it should be pointed out that the RCM feature for the proposed mechanism is independent with the inputs of the mechanism as long as the proposed mechanism satisfies the two conditions discussed above. In addition, RCM mechanisms with similarly topology but different geometric constraint as the one illustrated in Fig. 6 can also be obtained. The famous external positioning mechanism named

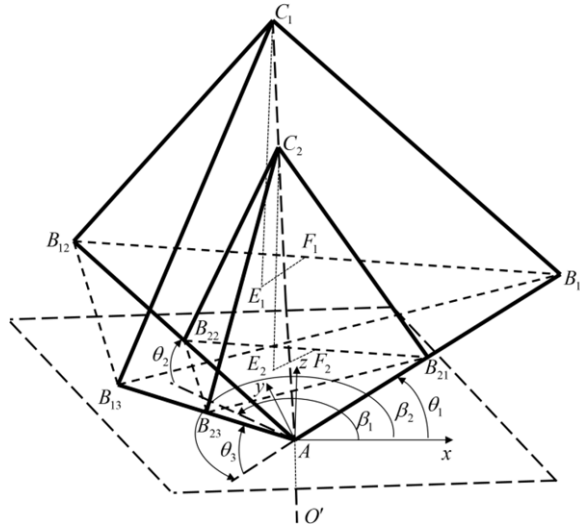


Figure 7. The kinematic model of the RCM mechanism based on two Delta linkages.

Dion is proposed by Ricardo et al. for robotic single port surgery [35] is a typical application example of this kind of RCM mechanism.

4. Forward kinematics and workspace of the proposed spatial RCM mechanism

Although it is easy to get the closed-form mathematical solution of the inverse kinematic problem for a parallel manipulator, the forward kinematic problem lacks a closed-form solution, due to the number of equations is less than the number of unknowns and the high degree of nonlinearity in the kinematic formulations [37]. The forward kinematic problem has posed a difficult problem for parallel manipulator researchers. In each of the proposed spatial RCM mechanisms, there are two parallel mechanisms, i.e., the two Delta linkages, that are coupled with remote center-of-motion each other, which makes the constraint even more complex. Therefore, it is essential to solve the forward kinematic problem to find the final position and orientation under a given set of joint angles and dimensional parameters. This can be used for monitoring the running status of an MIS surgical robot based on the proposed RCM mechanism.

4.1. Forward kinematic analysis

To carry out the forward kinematic analysis, the mathematical model of the mechanism is established, as shown in Fig. 7. In this model, the coordinate system A – xyz is the reference coordinate system. The x-axis coincides with the projection of the link AB₁₁ on the horizontal plane, z-axis points upward, and the y-axis complies with the right-hand rule. The values of the dimensional parameters are defined as follows: The length of link AB_{1j} (j = 1, 2, 3) is l_i, the length of link AB_{2i} is kl_i (0 < k ≤ 1), the length of link B_{2i}C₂ is l_{2i}, the length of link B_{1i}C₁ is l_{1i}, and the length of the End-link is l.

Since the End-link, usually is the surgical tool in a MIS robot, has a fixed value of length, the position of at the end of the End-link, i.e., point O', can be expressed by the position of points C₁ and point C₂ as

$$r_{O'} = r_{C1} - l \left(\frac{r_{C1} - r_{C2}}{\|r_{C1} - r_{C2}\|} \right) \tag{9}$$

where r_{O'} is the position vector of reference point O', r_{C1}, and r_{C2} denote the position vectors of points C₁ and C₂, respectively.

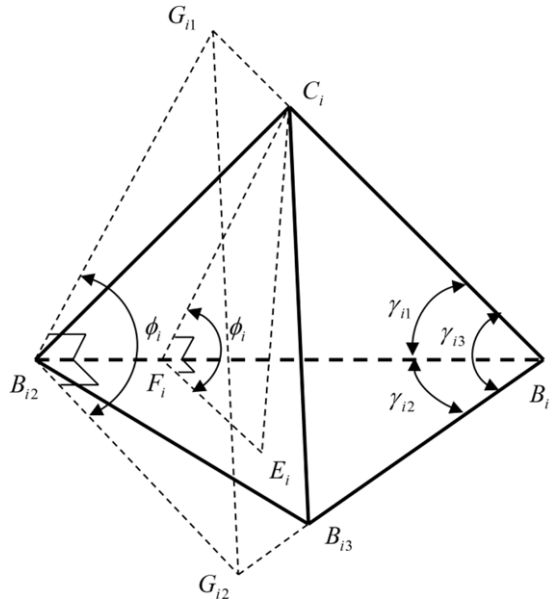


Figure 8. The mathematic model of the tetrahedron.

Then the kinematic analysis of the mechanism is equivalent to find the final positions of point C_1 and point C_2 under a given set of input joint angles, i.e., $\theta_1, \theta_2,$ and θ_3 of the three proximal links, as shown in Fig. 8. To carry out the calculation, two auxiliary lines are employed, they are lines C_1E_1 and C_2E_2 (see Fig. 7), which are perpendicular to plane $\pi B_{11}B_{12}B_{13}$ and plane $\pi B_{21}B_{22}B_{23}$, respectively. Then the position vectors of points C_1 and C_2 can be expressed as

$$\mathbf{r}_{C1} = \mathbf{r}_{E1} + \overline{E_1C_1} \tag{10}$$

$$\mathbf{r}_{C2} = \mathbf{r}_{E2} + \overline{E_2C_2} \tag{11}$$

where \mathbf{r}_{E1} and \mathbf{r}_{E2} are the position vectors of points E_1 and E_2 expressed in the reference coordinate system $A - xyz$. The coordinates of point B_{ij} ($i = 1, 2; j = 1, 2, 3$) can be determined by the input joint angles as

$$\mathbf{r}_{B1j} = l_j \text{Rot}(z, \beta_{(j-1)}) \text{Rot}(y, -\theta_j) \mathbf{e}_1 \tag{12}$$

$$\mathbf{r}_{B2j} = k_j l_j \text{Rot}(z, \beta_{(j-1)}) \text{Rot}(y, -\theta_j) \mathbf{e}_1 \tag{13}$$

where $\beta_{(j-1)}$ is the dimensional parameter, it is the angle of the projections of link AB_{ij} and link $AB_{i(j+1)}$ on the horizontal plane, and $\beta_0 = 0, \beta_1 \neq \beta_2$ and $\beta_0 + \beta_1 + \beta_2 = 2\pi$. In addition,

$$\text{Rot}(z, \beta_{(j-1)}) = \begin{bmatrix} \cos \beta_{(j-1)} & -\sin \beta_{(j-1)} & 0 \\ \sin \beta_{(j-1)} & \cos \beta_{(j-1)} & 0 \\ 0 & 0 & 1 \end{bmatrix}, \text{Rot}(y, -\theta_j) = \begin{bmatrix} \cos(-\theta_j) & 0 & \sin(-\theta_j) \\ 0 & 1 & 0 \\ -\sin(-\theta_j) & 0 & \cos(-\theta_j) \end{bmatrix}, \text{ and}$$

$$\mathbf{e}_1 = \begin{bmatrix} 1 \\ 0 \\ 0 \end{bmatrix}.$$

So far, all the lengths of the links in tetrahedrons $C_1 - B_{11}B_{12}B_{13}, C_2 - B_{21}B_{22}B_{23}, A - B_{11}B_{12}B_{13},$ and $A - B_{21}B_{22}B_{23}$ are known. Then, $\overline{E_1C_1}$ and $\overline{E_2C_2}$ can be calculated in $C_1 - B_{11}B_{12}B_{13}$ and $C_2 - B_{21}B_{22}B_{23}$, respectively, while $\overline{AE_1}$ and $\overline{AE_2}$ can be calculated in $A - B_{11}B_{12}B_{13}$ and $A - B_{21}B_{22}B_{23}$, respectively. Let

us solve the expression of $\overline{E_1C_1}$ and $\overline{E_2C_2}$ first. Their directional vectors can be obtained by

$$\mathbf{n}_{\overline{E_1C_1}} = \frac{\overline{B_{11}B_{12}} \times \overline{B_{11}B_{13}}}{\|\overline{B_{11}B_{12}} \times \overline{B_{11}B_{13}}\|} \tag{14}$$

$$\mathbf{n}_{\overline{E_2C_2}} = \frac{\overline{B_{21}B_{22}} \times \overline{B_{21}B_{23}}}{\|\overline{B_{21}B_{22}} \times \overline{B_{21}B_{23}}\|} \tag{15}$$

where $\overline{B_{11}B_{12}} = \mathbf{r}_{B_{12}} - \mathbf{r}_{B_{11}}$, $\overline{B_{11}B_{13}} = \mathbf{r}_{B_{13}} - \mathbf{r}_{B_{11}}$, $\overline{B_{21}B_{22}} = \mathbf{r}_{B_{22}} - \mathbf{r}_{B_{21}}$, and $\overline{B_{21}B_{23}} = \mathbf{r}_{B_{23}} - \mathbf{r}_{B_{21}}$.

To solve the length of $\overline{E_iC_i}$ which is perpendicular to the plane $\pi B_{i1}B_{i2}B_{i3}$, the mathematic model of the tetrahedron is established, as shown in Fig. 8. The thin-dotted lines in the model are the auxiliary lines and both of the two lines $B_{i2}G_{i1}$ and $B_{i2}G_{i2}$ are perpendicular with the line $B_{i1}B_{i2}$. Line $G_{i1}B_{i2}$ locates in the plane $\pi C_iB_{i1}B_{i2}$, while the line $B_{i2}G_{i1}$ locates in the plane $\pi B_{i1}B_{i2}B_{i3}$. According to cosine theorem, γ_{i1} which is the angle formed by line C_iB_{i1} and the line $B_{i1}B_{i2}$ can be calculated, it is

$$\gamma_{i1} = \arccos \frac{\|\overline{B_{i1}C_i}\|^2 + \|\overline{B_{i1}B_{i2}}\|^2 - \|\overline{B_{i2}C_i}\|^2}{2 \|\overline{B_{i1}C_i}\| \|\overline{B_{i1}B_{i2}}\|} \tag{16}$$

Then the length of $\overline{B_{i2}G_{i1}}$ can be solved by

$$\|\overline{B_{i2}G_{i1}}\| = \|\overline{B_{i1}B_{i2}}\| \tan \gamma_{i1} \tag{17}$$

By using same method, the length of $\overline{B_{i2}G_{i2}}$ can be obtained

$$\|\overline{B_{i2}G_{i2}}\| = \|\overline{B_{i1}B_{i2}}\| \tan \gamma_{i2} \tag{18}$$

where $\gamma_{i2} = \arccos \frac{\|\overline{B_{i1}B_{i2}}\|^2 + \|\overline{B_{i1}B_{i3}}\|^2 - \|\overline{B_{i2}B_{i3}}\|^2}{2 \|\overline{B_{i1}B_{i2}}\| \|\overline{B_{i1}B_{i3}}\|}$.

The length of $\|\overline{G_{i2}G_{i1}}\|$ can be calculated by

$$\|\overline{G_{i2}G_{i1}}\| = \sqrt{\|\overline{B_{i1}G_{i1}}\|^2 + \|\overline{B_{i1}G_{i2}}\|^2 - 2 \|\overline{B_{i1}G_{i1}}\| \cdot \|\overline{B_{i1}G_{i2}}\| \cos \gamma_{i3}} \tag{19}$$

where $\cos \gamma_{i3} = \frac{\|\overline{B_{i1}C_i}\|^2 + \|\overline{B_{i1}B_{i3}}\|^2 - \|\overline{B_{i3}C_i}\|^2}{2 \|\overline{B_{i1}C_i}\| \|\overline{B_{i1}B_{i3}}\|}$, $\|\overline{B_{i1}G_{i1}}\| = \frac{\|\overline{B_{i1}B_{i2}}\|}{\cos \gamma_{i1}}$, and $\|\overline{B_{i1}G_{i2}}\| = \frac{\|\overline{B_{i1}B_{i2}}\|}{\cos \gamma_{i2}}$.

Then the angle form by plane $C_iB_{i1}B_{i2}$ and plane $B_{i1}B_{i2}B_{i3}$ can be calculated by

$$\phi_i = \arccos \frac{\|\overline{B_{i2}G_{i1}}\|^2 + \|\overline{B_{i2}G_{i2}}\|^2 - \|\overline{G_{i2}G_{i1}}\|^2}{2 \|\overline{B_{i2}G_{i1}}\| \|\overline{B_{i2}G_{i2}}\|} \tag{20}$$

Then the length of $\overline{E_iC_i}$ can be calculated consequently, it is

$$\|\overline{E_iC_i}\| = \|\overline{C_iF_i}\| \sin \phi_i \tag{21}$$

where $C_iF_i \perp B_{i1}B_{i2}$ and $\|\overline{C_iF_i}\| = \|\overline{B_{i1}C_i}\| \sin \gamma_{i1}$. Till now, the directional vector and the length of $\overline{E_iC_i}$ are solved.

The position vector of point E_i can be calculated in tetrahedrons $A - B_{i1}B_{i2}B_{i3}$

$$\mathbf{r}_{E_i} = \mathbf{r}_{B_{i1}} + \overline{B_{i1}F_i} + \overline{F_iE_i} \tag{22}$$

where $\overline{B_{i1}F_i} = \|\overline{B_{i1}C_i}\| \cos \gamma_{i1} \frac{\overline{B_{i1}B_{i2}}}{\|\overline{B_{i1}B_{i2}}\|}$, $\overline{F_iE_i} = (\|\overline{C_iF_i}\| \cos \phi_i) \frac{\overline{E_iC_i} \times \overline{B_{i1}B_{i2}}}{\|\overline{E_iC_i} \times \overline{B_{i1}B_{i2}}\|}$.

Since all the unknowns are expressed by the dimensional parameters and the input joint angles of the mechanism, the positions of points C_1 and C_2 can be derived by Eqs. (10), (11), (14), (15), (21), and (22). And consequently, the forward position analysis result, the final position of the reference point O' at the end of the End-link, can be derived by Eq. (9). It can be seen that the unique solution of the forward kinematic problem can be obtained based on the employed geometrical analysis method. One advantage of this process is that it can avoid the choosing procedure in the analytical technique, which may yield multiple solutions. Another advantage is that it can also avoid the time-consuming iteration calculation in the forward kinematic analysis based on numerical techniques.

Table I. The dimensional parameters of the research object.

AB_{11}	AB_{12}	AB_{13}	$B_{11}C_1$	$B_{12}C_1$	$B_{13}C_1$	k	l	β_0	β_1	β_2
180 mm	200 mm	220 mm	220 mm	200 mm	180 mm	0.5	350 mm	0°	120°	240°

Table II. The dimensional parameters of the research object.

Given position (mm)	Angular positions (°)	Calculated position (mm)
(92.74, 29.13, -112.82)	$\theta_1 = 59.55, \theta_2 = 30.09, \theta_3 = 12.91$	(92.7373, 29.1237, -112.8237)
(-20.19, 28.75, -76.28)	$\theta_1 = 22.67, \theta_2 = 66.37, \theta_3 = 42.26$	(-20.1874, 28.7511, -76.2667)
(-14.86, -92.46, -182.53)	$\theta_1 = 1.49, \theta_2 = 0.52, \theta_3 = 61.63$	(-14.3471, -92.0539, -183.3742)



Figure 9. Different configurations of the mechanism with the given positions in Table II.

4.2. Numerical simulation and verification

To verify the validity of the forward kinematic calculation process, a numerical example is employed in this section. The RCM mechanism is generated based on the second condition, which means the corresponding distal links in the two Delta mechanisms are parallel to each other, the forward kinematics of which is more complicated than the first condition. The dimensional parameters in this example are listed in Table I.

The verification process is that a set of reference positions whose values and the corresponding input joint angles were measured from SolidWorks® software were given first. After that, the forward kinematic analysis was carried out to solve the positions of the reference point based on the joint angles. Then comparison between the given reference positions and the positions obtained through forward kinematic calculation was carried out to check the accuracy of the procedure. The comparison results are listed in Table II. It can be seen that the forward position calculation method is effective. For the third calculation, however, the error between the given position and the calculated position is large. The reason is that the absolute values of two angular positions are small, which makes the relative measured errors of these two angles large, and consequently results in a relative larger calculation error. The configurations of the mechanism with the 3 given angular positions are shown in Fig. 9.

4.3. Workspace analysis

In the process of motion, the boundary of workspace is determined by the limit position of rotating joint. Number the outer circle joints in sequence as shown in Fig. 10(a), and the diagonal joints of each parallelogram interfere at the same time. When joint 1 reaches the limit position, the joints in the four circles reach the limit position at the same time. Drag the moving platform clockwise in a plane, and every two pairs of joints 1 and 4, 1 and 6, 6 and 3, 3 and 2, 2 and 5, 5 and 4 interfere at the same time. The moving track of the moving platform is a regular hexagon, and the sides of the hexagon are equal in different planes. Figure 10(a) shows the interference state of joints 1 and 4. The moving

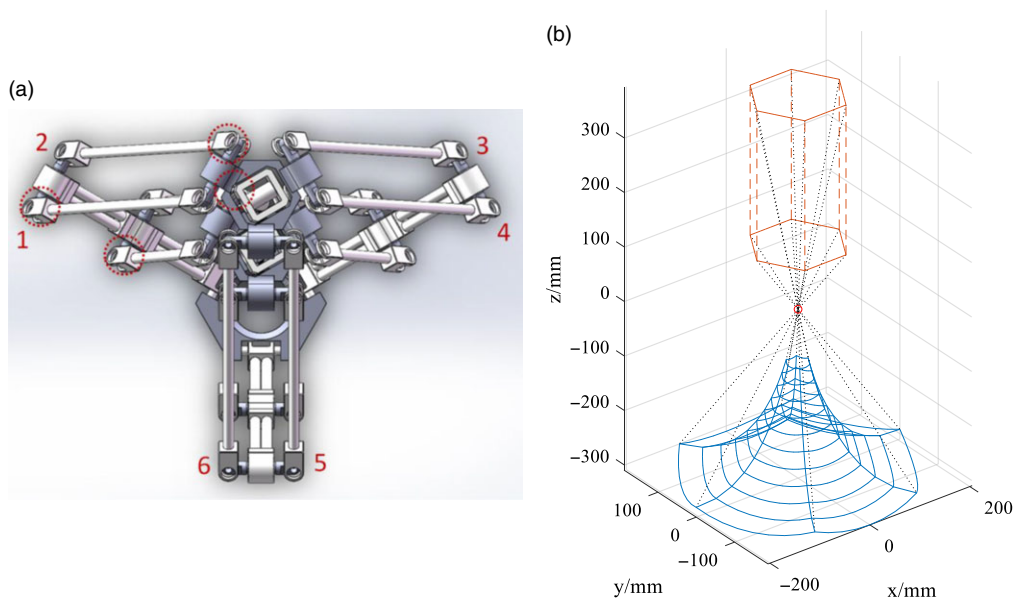


Figure 10. Interference configuration and workspace of the proposed mechanism.

range of the moving platform in the vertical direction is 119–393 mm, from which the working space can be calculated. As shown in Fig. 10(b), the orange hexagonal prism is the motion range of the top moving platform, and the blue part is the space that can be reached at the end of the instrument. When the insertion depth of the instrument is the maximum, the maximum deflection angle is 62.6° . When the insertion depth of the instrument is the smallest, the maximum deflection angle is 23.7° . Obviously, the rotation range of the rotating joint can be increased by optimizing the connecting rod structure, so as to effectively increase the adjustment angle of the RCM mechanism. Chen et al. proposed a parallel RCM manipulator with a workspace of 60° and explained the reliability of this workspace by analyzing the human body size [39].

4.4. Prototype manufacturing and principle verification

To verify the correctness of the proposed mechanism, a prototype of the mechanism was fabricated, as shown in Fig. 11(a). All the linkages have been manufactured by 3D printing, and all the revolute joints are connected by bearings. The parameters of the prototype are identical with those in Table I. The diameter of the End-link is 4.3 mm. A laser pointer with green laser was utilized to point the remote center of the prototype. Once the End-link cross the remote center, the green spot will be observed on the End-link.

Different configurations have been reached manually, and the positions of End-link relative the remote center have been captured. For each configuration in Fig. 11, the End-link is always with the green spot, verifying the motion of the End-link is restrained by the remote center.

5. Conclusion

A class of spatial RCM mechanisms is introduced in this paper. And the essential conditions that make the mechanism be an RCM mechanism are proved. Due to the parallel kinematic configuration, the proposed mechanisms are quite suitable to be used in the areas that require the surgical robots with high load capacity. The proposed RCM mechanism is promising to be used as a guidance device in robot

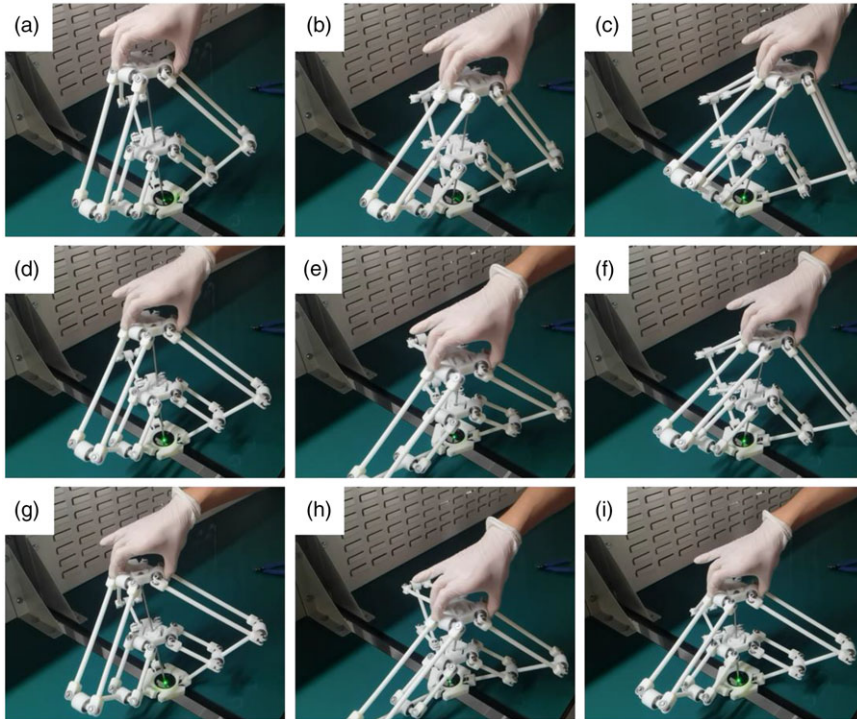


Figure 11. Different configurations of the proposed prototype.

assisting needle insertion applications or be used as an external positioner in robotic single-port surgeries. To satisfy the real-time monitoring requirement during robotic surgeries, the forward kinematic problem of the proposed mechanism was solved based on geometrical method. Based on this method, the unique forward kinematic solution of the spatial RCM mechanism can be obtained. This technique avoids the choosing the valid result from the multiple solutions procedures in an analytical calculation or implementing the computational expensive iterative numerical methods. Further research will be focused on quantitative evaluation of the motion accuracy based on alignment sensor, stiffness analysis, and prototype design for MIS.

Author contributions. Yuan Bian and Jianmin Li conceived and designed the study, Jianchang Zhao made the prototype for experiment, Jianmin Li and Jinhua Li wrote the paper, and Guowu Wei reviewed and edited the manuscript.

Financial support. This paper is supported by grants from National Natural Science Foundation of China under grants 52122501, 51875394, and 52075277.

Conflicts of interest. The authors declare that there is no conflict of interest.

Ethical considerations. No ethical approval was required.

References

- [1] J. S. Dai, "Surgical robotics and its development and progress," *Robotica* **28**, 161 (2010).
- [2] G. S. Guthart and J. K. Salisbury Jr., "The Intuitive Telesurgery System: Overview and Application," **In: Proceedings of the 2000 IEEE International Conference on Robotics and Automation**, San Francisco, CA (2000) pp. 618–621.
- [3] J. M. Li, G. K. Zhang, Y. Xing, H. B. Liu and S. X. Wang, "A class of 2-degree-of-freedom planar remote center-of-motion mechanisms based on virtual parallelograms," *Trans. ASME J. Mech. Robot.* **6**(3), 031014 (2014).

- [4] U. Hagn, R. Konietschke, A. Tobergte, M. Nickl, S. Jörg, B. Kübler, G. Passig, M. Gröger, F. Fröhlich, U. Seibold, L. Le-Tien, A. Albu-Schäffer, A. Nothhelfer, F. Hacker, M. Grebenstein and G. Hirzinger, "DLR MiroSurge - A versatile system for research in endoscopic telesurgery," *Int. J. Comput. Assist. Radiol. Surg.* **5**(2), 183–193 (2010).
- [5] D. Pisla, A. Szilaghyi, C. Waida and N. Plitea, "Kinematics and workspace modeling of a new hybrid robot used in minimally invasive surgery," *Robot. Comput. Integr. Manuf.* **29**(2), 463–474 (2013).
- [6] D. Pisla, B. Gherman, C. Waida, M. Suciuc and N. Plitea, "An active hybrid parallel robot for minimally invasive surgery," *Robot. Comput. Integr. Manuf.* **29**(4), 203–221 (2013).
- [7] B. Gherman, D. Pisla, C. Waida and N. Plitea, "Development of inverse dynamic model for a surgical hybrid parallel robot with equivalent lumped masses," *Robot. Comput. Integr. Manuf.* **28**(3), 402–415 (2012).
- [8] M. Ghodoussi, S. E. Butner and Y. L. Wang, "Robotic Surgery - The Transatlantic Case," **In:** Proceedings 2002 IEEE International Conference on Robotics and Automation, Washington, DC (2002) pp. 1882–1888.
- [9] W. Wang, J. Li and S. Wang, "System design and animal experiment study of a novel minimally invasive surgical robot," *Int. J. Med. Robot. Comput. Assist. Surg.* **12**(1), 73–84 (2016).
- [10] R. C. O. Locke and R. V. Patel, "Optimal Remote Center-of-Motion Location for Robotics-Assisted Minimally Invasive Surgery," **In:** Proceedings of the IEEE International Conference on Robotics and Automation, Rome, Italy (2007) pp. 1900–1905.
- [11] R. H. Taylor and D. Stoianovici, "Medical robotics in computer-integrated surgery," *IEEE Trans. Robot. Autom.* **19**(5), 765–781 (2003).
- [12] J-U. Stolzenburg, P. Kallidonis, D. Minh, A. Dietel, T. Häfner, D. Dimitriou, A. Al-Aown, I. Kyriazis and E. N. Liatsikos, "Endoscopic extraperitoneal radical prostatectomy: Evolution of the technique and experience with 2400 cases," *J. Endourol.* **23**(9), 1467–1472 (2009).
- [13] S. Voros, G. P. Haber, J. F. Menudet, J. A. Long and P. Cinquin, "ViKY robotic scope holder: Initial clinical experience and preliminary results using instrument tracking," *IEEE ASME Trans. Mechatron.* **15**(6), 879–886 (2010).
- [14] X. L. Zhang and C. A. Nelson, "Kinematic analysis and optimization of a novel robot for surgical tool manipulation," *ASME J. Med. Dev.* **2**(2), 021003 (2008).
- [15] Z. Nabil and M. Guillaume, "Mechatronic design of a new robot for force control in minimally invasive surgery," *IEEE ASME Trans. Mechatron.* **2**(2), 143–153 (2007).
- [16] J. R. Shi, M. Pascal, P. Viviane, M. Guillaume and S. X. Wang, "Preliminary Results on the Design of a Novel Laparoscopic Manipulator," **In:** Proceedings of the 11th World Congress in Mechanisms and Machine Science, Tianjin, China (2003) pp. 1811–1815.
- [17] M. J. H. Lum, D. C. W. Friedman, G. Sankaranarayanan, H. King, K. Fodero, R. Leuschke, B. Hannaford, J. Rosen and M. N. Sinanan, "The RAVEN: Design and validation of a telesurgery system," *Int. J. Robot. Res.* **28**(9), 1183–1197 (2009).
- [18] M. Zoppi, D. Zlatanov and C. M. Gosselin, "Analytical kinematics models and special geometries of a class of 4-DOF parallel mechanisms," *IEEE Trans. Robot.* **21**(6), 1046–1055 (2005).
- [19] R. H. Taylor, J. Funda, B. Eldridge, S. Gomory, K. Gruben, D. LaRose, M. Talamini, L. Kavoussi and J. Anderson, "A telerobotic assistant for laparoscopic surgery," *Eng. Med. Biol. Mag.* **14**(3), 279–288 (1995).
- [20] Z. Nawrat and P. Kostka, "Polish cardio-robot 'RobIn Heart'. System, description and technical evaluation," *Int. J. Med. Robot. Comput. Assist. Surg.* **2**, 36–44 (2006).
- [21] J. Rosen, J. D. Brown, L. Chang, M. Barreca, M. Sinanan and B. Hannaford, "The BlueDRAGON – A system for Measuring the Kinematics and the Dynamics of Minimally Invasive Surgical Tools In-Vivo," **In:** International Conference on Robotics and Automation, Washington, DC (2002) pp. 1876–1881.
- [22] R. H. Taylor, P. Jensen, L. Whitcomb, A. Barnes, R. Kumar, D. Stoianovici, P. Gupta, Z. X. Wang, E. de Juan and L. Kavoussi, "A Steady-Hand Robotic System for Microsurgical Augmentation," **In:** The Second International Conference on Medical Image Computing and Computer-Assisted Intervention, Cambridge, UK, vol. **1679** (1999) pp. 1031–1041.
- [23] W. C. Nowlin, G. S. Guthart, J. K. Salisbury and G. D. Niemeyer, "Repositioning and Reorientation of Master/Slave Relationship in Minimally Invasive Telesurgery," U. S. Patent No. US7087049B2 (2006).
- [24] N. X. Zhou, Z. Y. Zhu, J. Z. Chen, Q. D. Liu, T. Zhang and Z. F. Chen, "Delayed right hemihepatectomy followed by right-hepatic vascular control both by da Vinci robotic surgery to a patient of HilarCholangiocarcinoma with deep jaundice," *Robot. Surg.* **1**, 90–97 (2011).
- [25] G-P. Haber, M. A. White, R. Autorino, P. F. Escobar, M. D. Kroh, S. Chalikhonda, R. Khanna, S. Forest, B. Yang, F. Altunrende, R. J. Stein and J. H. Kaouk, "Novel robotic da Vinci instruments for laparoendoscopic single-site surgery," *Urology* **76**(6), 1279–1282 (2010).
- [26] E. J. Hanly and M. A. Talamini, "Robotic abdominal surgery," *Am. J. Surg.* **188**(4), 19S–26S (2004).
- [27] G. H. Zong, X. Pei, J. J. Yu and S. S. Bi, "Classification and type synthesis of 1-DOF remote center of motion mechanisms," *Mech. Mach. Theory* **43**(12), 1585–1595 (2008).
- [28] J. M. Li, S. X. Wang, X. F. Wang and C. He, "Optimization of a novel mechanism for a minimally invasive surgery robot," *Int. J. Med. Robot. Comput. Assist. Surg.* **6**, 83–90 (2010).
- [29] J. M. Li, S. X. Wang, X. F. Wang, C. He and L. A. Zhang, "Development of a Novel Mechanism for Minimally Invasive Surgery," **In:** International Conference on Robotics and Biomimetics, Tianjin, China (2010) pp. 1370–1375.
- [30] C. H. Kuo, J. S. Dai and P. Pasgupta, "Kinematic design considerations for minimally invasive surgical robots: An overview," *Int. J. Med. Robot. Comput. Assist. Surg.* **8**(2), 127–145 (2012).
- [31] R. Beira, L. Santos-Carreras, A. Sengül, E. Samur, R. Clavel and H. Bleuler, "An external positioning mechanism for robotic surgery," *J. Syst. Des. Dyn.* **5**(5), 1094–1105 (2011).

- [32] J. M. Li, G. K. Zhang, A. Muller and S. X. Wang, "A family of remote center of motion mechanisms based on intersecting motion planes," *Trans. ASME J. Mech. Des.* **135**(9), 091009 (2013).
- [33] C. H. Kuo and J. S. Dai, "Kinematics of a fully decoupled remoter center-of-motion parallel manipulator for minimally invasive surgery," *Trans. ASME J. Med. Dev.* **6**(2), 021008 (2012).
- [34] H. Long, Y. Yang, X. Jingjing and S. Peng, "Type synthesis of 1R1T remote center of motion mechanisms based on pantograph mechanisms," *J. Mech. Des.* **138**(1), 014501 (2016).
- [35] R. Clavel, "Device for the Movement and Positioning of an Element in Space," US Patent 4976582 (1990).
- [36] B. Ricardo, S. C. Laura, S. Ali, S. Evren, C. Reymand and B. Hannes, "An external positioning mechanism for robotic surgery," *J. Syst. Des. Dyn.* **5**(5), 1094–1105 (2011).
- [37] P. J. Parikh and S. S. Y. Lam, "A hybrid strategy to solve the forward kinematics problem in parallel manipulators," *IEEE Trans. Robot.* **21**(1), 18–25 (2005).
- [38] J. S. Dai, Z. Huang and H. Lipkin, "Mobility of overconstrained parallel mechanisms," *Trans. ASME J. Mech. Des.* **128**(1), 220–229 (2006).
- [39] G. Chen, J. Wang, H. Wang, C. Chen, V. Parenti-Castelli and J. Angeles, "Design and validation of a spatial two-limb 3R1T parallel manipulator with remote center-of-motion," *Mech. Mach. Theory* **149**(2), 103807 (2020).